VOL. 12, NO. 3, FEBRUARY 2017 ISSN 1819-6608
ARPN Journal of Engineering and Applied Sciences

www.arpnjournals.com

INSTABILITY OF A SHOCK WAVE OVER A BACKWARD FACING RAMP

Alexander Kuzmin and Konstantin Babarykin
Department of Fluid Dynamics, St. Petersburg State University, Russia
E-Mail: a.kuzmin@spbu.ru

ABSTRACT

The turbulent transonic flow over a wall with an expansion corner and ramp is studied numerically at free-stream Mach numbers from 1.11 to 1.28. A shock wave forms in front of a horizontal plate or bar located above the ramp. Solutions of the Reynolds-averaged Navier-Stokes equations are obtained on fine meshes with a finite-volume solver of second-order accuracy. The solutions demonstrate instability of the shock position at certain free-stream Mach numbers, which depend on the streamwise location of the plate/bar with respect to the ramp. The flow behavior under steady and unsteady perturbations in the free stream is analyzed. Also positions of the shock as functions of the ramp slope are studied.

Keywords: transonic flow, shock waves, instability, bifurcation, hysteresis.

1. INTRODUCTION

In the 1990s and 2000s, numerical simulations of transonic flows revealed instability of double supersonic regions on airfoils comprising a flat or nearly flat arc [1-3]. The instability is caused by an interaction between the shock wave, which terminates the bow supersonic region, and the sonic line, which is a front of the rear supersonic region. The spacing between the shock and sonic line decreases as the free-stream Mach number increases; however, it cannot vanish because the shock and sonic line cannot have a common point on the airfoil. Therefore, if M_∞ exceeds a certain value, then the shock jumps downstream and creates a coalescence of the bow and rear supersonic regions. In the 3D flow over wings, the supersonic regions may coalesce either gradually or abruptly, depending on the wing sweep angle [4].

The same type of instability takes place in channel flows where the sonic line arises over an expansion corner of a wall, while the shock is formed due to a bend of another wall. A dependence of the flow instability and bifurcation on the velocity profile given at the inlet of a divergent channel was studied in [5]. Effects of the angle of attack on the shock bifurcation in the entrance region of a simple intake were examined in [6]. In practice, such problems may occur, e.g., when a supersonic intake encounters variations of the incoming flow due to the atmospheric turbulence or a maneuvering flight of aircraft [7, 8].

In this paper, we study shock wave instability in front of a horizontal plate/bar located above a backward facing ramp. In contrast to [5], the computational domain involves a region ahead of the plate in order to capture the detached shock wave. We determine free-stream Mach numbers, streamwise locations of the ramp and expansion corner angles, at which the shock position is extremely sensitive to small perturbations.

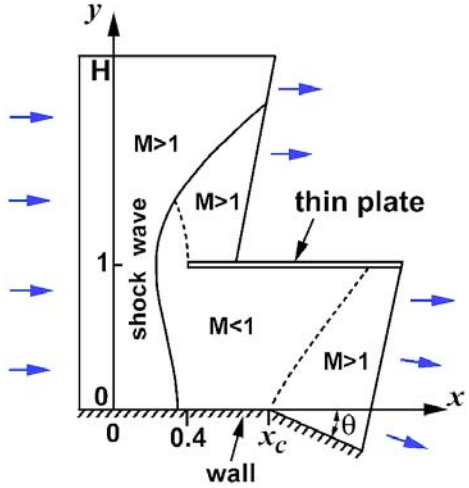

Figure-1. Sketch of the computational domain.

2. FORMULATION OF THE PROBLEM

In Sections 2-5, we consider a solid wall with a break of 16° given by the expressions

$$y=0 \text{ at } 0\le x\le x_c\,;\quad y=-(x-x_c)\tan(16°) \text{ at } x_c<x\le x_{out}. \qquad (1)$$

A horizontal plate of 0.006 m thickness and 0.33 m length is placed above the wall in such a way that its lower surface coincides with the segment y=0.3 m, $0.12\le x$, m ≤ 0.45. In what follows, the Cartesian coordinates (x,y,z) are non-dimensionalized by the height h=0.3 m, so that the plate occupies the region

$$1<y<1.02,\ 0.4<x<1.5, \qquad (2)$$

see Figure-1. The left boundary of the computational domain is set to x=0, $0<y<H$. The upper boundary is remote at a distance H=6 from the wall in order to eliminate its influence on the flow in the plate/wall region. The outlet boundary is constituted by two segments with the endpoints

x=0.7, y=1.02 ; x=1.5, y=H , (3)

and

x= x_{out} , y= y_{out} ; x=1.5, y=1 , (4)

where x_{out} =1.24, y_{out} = -(x_{out} -x_c) tan(16°). The choice of the oblique segment (4) (instead of a vertical one) makes it possible to reduce the computational domain and avoid complications arising because of a boundary layer separation from the wall in the interval 1.24< x < 1.5.

At the outlet, we impose the condition of the supersonic flow regime. On the left boundary x=0, we prescribe the flow velocity, static pressure p_∞=100,000 N/m^2, and static temperature T_∞=250 K which determines the sound speed a_∞=317.02 m/s. The no-slip condition and vanishing heat flux are used on the wall and plate. Initial data are parameters of the uniform free stream. The air is treated as a perfect gas whose specific heat at constant pressure is 1004.4 J/(kg K) and the ratio of specific heats is 1.4. We adopt the value of 28.96 kg/kmol for the molar mass, and use the Sutherland formula for the molecular dynamic viscosity. The free-stream Mach numbers under consideration are 1.11 ≤ M_∞≤ 1.28; therefore, the Reynolds number based on M_∞ and the height h=0.3 m is about 8.7×10^6.

Solutions of the unsteady Reynolds-averaged Navier-Stokes equations were obtained with an ANSYS-15 CFX finite-volume solver, which is based on a numerical scheme of second-order accuracy. An implicit backward Euler scheme was employed for the time-accurate computations. We used a Shear Stress Transport k-ω turbulence model which is known to reasonably predict aerodynamic flows with boundary layer separations [9].

Numerical simulations of 2D flow were performed on hybrid computational meshes constituted by quadrangles in 39 layers on the plate and wall, and by triangles in the remaining region. The non-dimensional thickness y^+ of the first mesh layer on the plate and wall was less than 1. Apart from the boundary layer region, mesh nodes were clustered in vicinities of the expansion corner and shock wave. Test computations on uniformly refined meshes of approximately 10^5, 2×10^5, and 4×10^5 cells showed that a discrepancy between shock wave coordinates obtained on the second and third meshes did not exceed 1%. Global time steps of 10^{-6} s and 2×10^{-6} s yielded undistinguishable solutions. That is why we employed meshes of 2×10^5 cells and the time step of 2×10^{-6} s for the study of 2D transonic flow at various free-stream velocities. The root-mean-square CFL number (over mesh cells) was about 3.

Simulations of 3D flow were performed in a domain created by an extrusion of the 2D domain in the z-direction from z=0 up to z=1. An unstructured mesh was constituted by 3.2×10^6 prisms in 39 layers on the plate and wall, and by 18.1×10^6 tetrahedrons in the remaining region. The solver was verified by computation of a few commonly used 2D and 3D test cases, in particular, transonic flow in a channel of 184 cm length and 19 cm height with a circular-arc bump and a curved shock located on the bump [5, Figure-2].

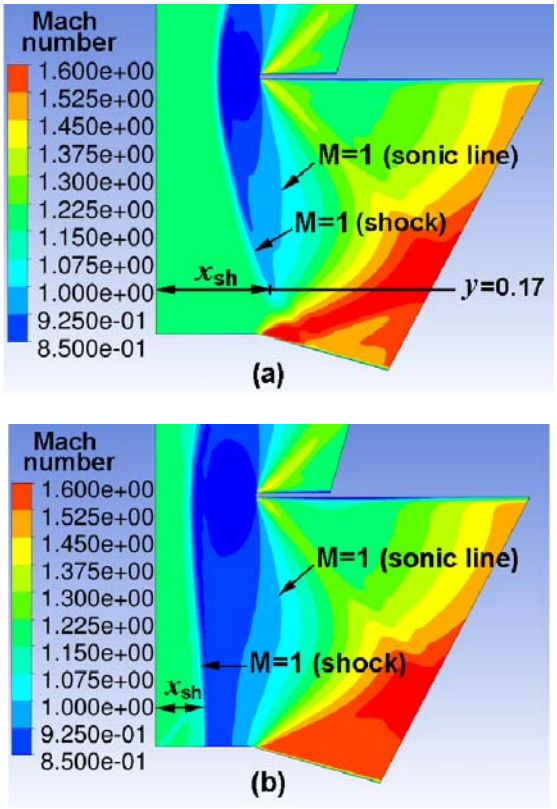

Figure-2. Mach number contours in the flow over the wall with the corner location x_c=0.4: a) M_∞=1.19, (b) M_∞=1.16.

3. STREAMWISE POSITIONS OF THE 2D SHOCK VERSUS M_∞ AT VARIOUS LOCATIONS OF THE EXPANSION CORNER

Let the free stream be uniform and parallel to the x-axis, so that the x- and y-components of the incoming flow velocity are

U_∞=M_∞ a_∞ , V_∞= 0 at x=0, 0<y< H. (5)

Computations of 2D flow in the band 1.14≤ M_∞ ≤1.28 demonstrated a convergence of the mean parameters of turbulent flow to steady states in less than 0.2 s of physical time.

For M_∞=1.19 and the expansion corner located at x_c=0.4, the steady flow field exhibits a curved shock, behind which the velocity is subsonic except for a small vicinity of the corner, see Figure-2a. The vicinity resides beneath the line y=0.17, so that there are intersections of the line with the V-shaped contour M(x,y)=1. The x-coordinate x_{sh} of the left intersection point is used hereafter to trace the streamwise position of the shock.

Numerical simulations demonstrated a shift of the shock position upstream with decreasing M_∞ step-by-step from 1.19 to 1.162, as indicated by dots on the upper

branch of curve 2 in Figure-3. If M_∞ is further decreased to 1.16, then the supersonic region splits, and a relaxation yields a steady flow with two supersonic regions separated by a subsonic zone (Figure-2b). The splitting is accompanied by a jump of the shock from the position x_{sh}=0.3333 to x_{sh}=0.2016. Further decrease of M_∞ to 1.142 causes a gradual displacement of the shock position upstream and an increase of the distance between the shock and the expansion corner. Inversely, when M_∞ increases from 1.142 to 1.16, the shock gradually shifts downstream, and x_{sh} increases from 0.0165 to 0.2016. After that, if M_∞ is further increased to 1.162, then the shock jumps to the position $x_{sh} \approx 0.336$.

For the expansion corner located at x_c=0.5, computations showed a similar behavior of the shock wave (curve 3 in Figure-3), though the jump of x_{sh} is smaller than that in the previous case.

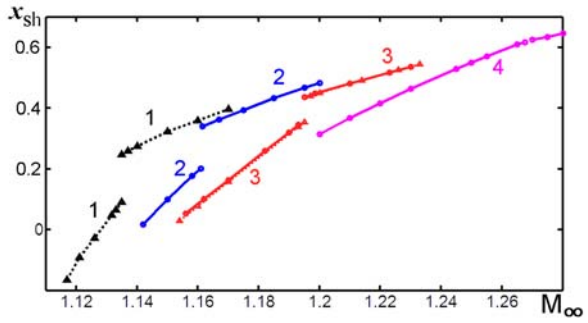

Figure-3. Shock wave coordinate x_{sh} at the height y=0.17 versus the free-stream Mach number M_∞ at various locations of the expansion corner: 1 – x_c=0.3, 2 – x_c=0.4, 3 – x_c=0.5, 4 – x_c=0.7. Dashed curves (indicated by the triangles) show the shock positions obtained in an enlarged computational domain.

If the expansion corner is placed at x_c=0.7, then the shock foot reaches the corner at larger values of M_∞. Figures 4a and 4b show that, with an increase of M_∞ from 1.23 to 1.255, the shock and sonic line approach each other inside the flow. At M_∞=1.268 they get into a contact, creating a local subsonic region near the wall (Figure-4c). Further increase of M_∞ entails shrinking the subsonic region, which eventually disappears and admits a gradual transition from the flow with a Mach stem to the flow with a shock wave terminated at the expansion corner (Figure-4d). As a consequence, curve 4 in Figure-3, which corresponds to x_c=0.7, is continuous.

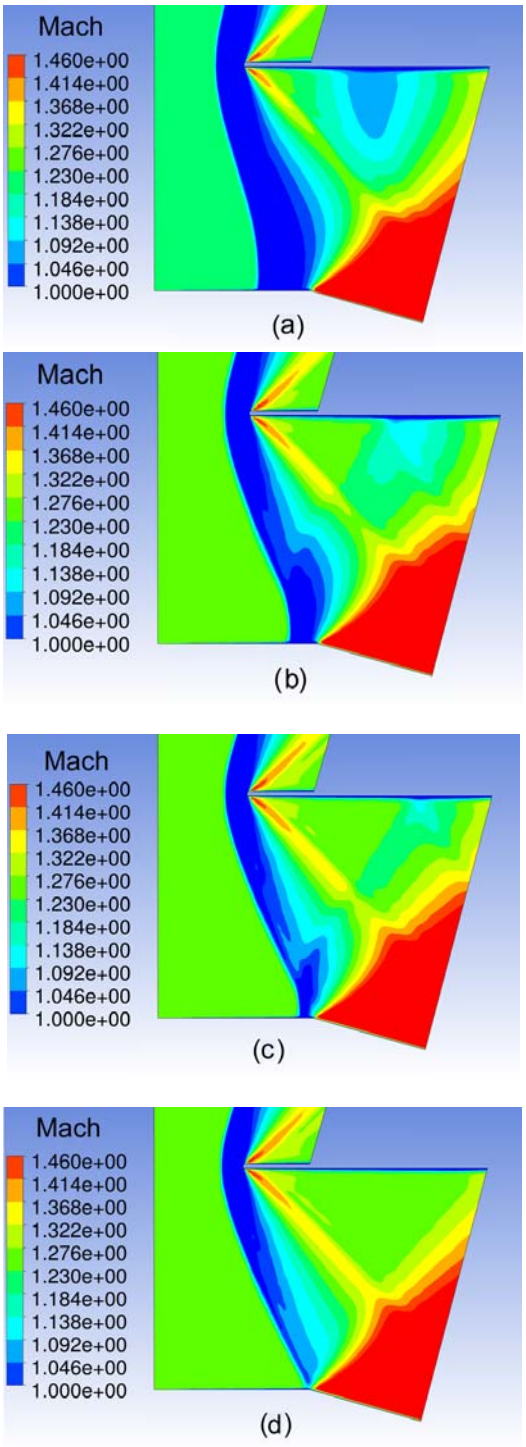

Figure-4. Shock wave positions at x_c=0.7 and (a) M_∞= 1.230, (b) M_∞ =1.255, (c) M_∞ =1.268, (d) M_∞ =1.270.

If $M_\infty<1.13$ and the coordinate x_c of the corner is 0.3, then the shock migrates upstream and hits the boundary $x=0$ of the computational domain. In this case, in order to capture the shock, we set the left boundary to $x= -0.3$ and prolong the wall to this coordinate. For the enlarged computational domain, a dependence of the shock wave position on M_∞ at $x_c=0.3$ is illustrated by curve 1 in Figure-3. In order to explore an effect of the expanded boundary layer (due to the longer wall), we recomputed the shock position in the enlarged domain for $x_c=0.5$. A comparison of the dashed and solid branches of curve 3 shows that the effect is negligible.

4. OSCILLATORY FREE-STREAM VELOCITY, $x_C=0.4$

Now we suppose that the Mach number of the incoming flow oscillates, while the velocity direction remains parallel to the x-axis,

$$U_\infty=M_\infty(t)\, a_\infty \ , \quad V_\infty= 0 \quad \text{at} \quad x=0, \quad 0<y<H, \qquad (6)$$

where $M_\infty(t)= (1+\delta \sin(2\pi t/T))\, M_{mid}$.

If $M_{mid}=1.16$ and $\delta=0.00862$, then $M_\infty(t)$ oscillates between 1.15 and 1.17. For the period $T=0.05$ s, the numerical simulation shows shock position oscillations in the interval

$x_{sh,min}= 0.149 \le x_{sh} \le x_{sh,max}= 0.250$,

which is shorter than the band $0.0997 \le x_{sh} \le 0.375$ determined by curve 2 in Figure-3 for the stationary values $M_\infty=1.15$ and $M_\infty=1.17$. This is explained by the insufficient time $T=0.05$ s for accomplishing the flow relaxation to steady states corresponding to different branches of curve 2. Meanwhile for the doubled period $T=0.1$ s computations showed oscillations of x_{sh} in the longer interval

$$0.120 \le x_{sh} \le 0.282. \qquad (7)$$

If now M_{mid} is increased to 1.17, so that $M_\infty(t)$ oscillates with the same $T=0.1$ s and the same amplitude between $M_\infty=1.16$ and $M_\infty=1.18$, then shock wave oscillations are halved as compared to (7):

$$0.329 \le x_{sh} \le 0.412.$$

This is explained by the fact that, during the full period of oscillations, the shock positions correspond to the upper branch of curve 2 in Fig. 3; therefore there are no abrupt changes of the flow pattern.

Finally, let the free-stream Mach be 1.17, while the angle of attack oscillates between -1° and +1°, i.e., the flow velocity components are

$U_\infty=M_\infty\, a_\infty \cos\alpha, \quad V_\infty= M_\infty\, a_\infty \sin\alpha, \quad \alpha= \sin(2\pi t/0.1)$,

instead of (6). Then computations demonstrate oscillations of the shock leg in a wide interval between the vicinity of expansion corner and the left boundary of the computational domain:

$$0.0756 \le x_{sh} \le 0.480.$$

This confirms a high sensitivity of the flow field to small perturbations at Mach numbers which are close to the discontinuity of curve 2 in Figure-3.

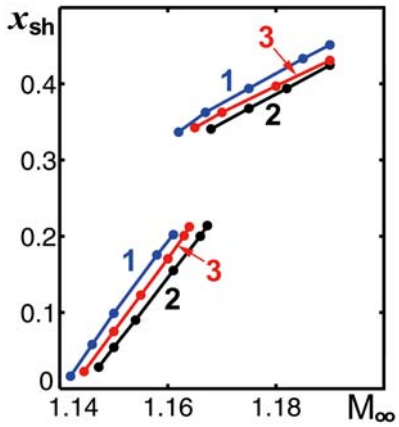

Figure-5. Shock wave coordinate x_{sh} versus M_∞ at $x_c=0.4$: 1 - 2D flow, 2 - 3D flow, 3 -D flow in which the plate (2) is replaced by the bar (8).

5. 3D FLOW COMPUTATIONS

In 3D flow simulations, the side boundaries $z=0$ and $z=1$ of the computational domain were split into two parts by the segments $y= 2.5x$, $0\le x\le 0.4$ and the plate depicted in Figure-1. Each of the lower parts is given by the expressions $y\le 2.5x$ at $0\le x\le 0.4$, $y\le 1.02$ at $0.4\le x\le x_{out}$ and is treated as a solid sidewall of a channel. The upper parts are endowed with a symmetry condition and considered as an interface between the flow in the domain $0<z<1$ and the ambient flow in domains $z<0$ and $z>1$. The incoming flow is parallel to the x-axis. For the expansion corner location $x_c=0.4$, the obtained shock positions are illustrated by curve 2 in Figure-5. The coordinate x_{sh} of 3D shock was calculated at the height $y=0.17$ in the midspan section of the channel $z=0.5$. Figures 6 and 7 show the shock and sonic surfaces locations for $M_\infty=1.16$. In addition to the sonic surface connecting the plate and corner region, Figure-6 demonstrates the sonic surface $M(x,y,z)=1$ in the boundary layers.

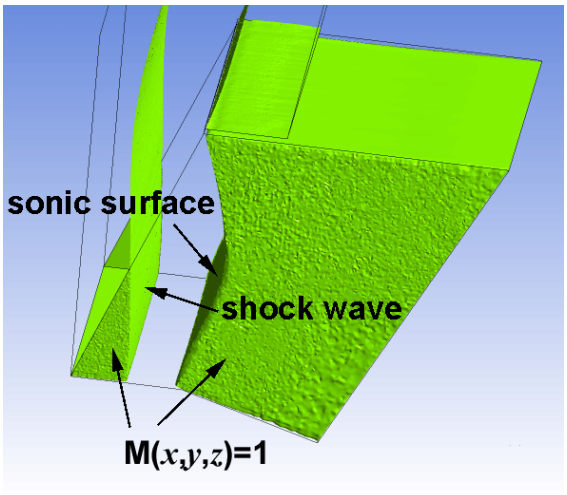

Figure-6. Surfaces M(x,y,z)=1 in the 3D flow at M_∞=1.16, x_c=0.4.

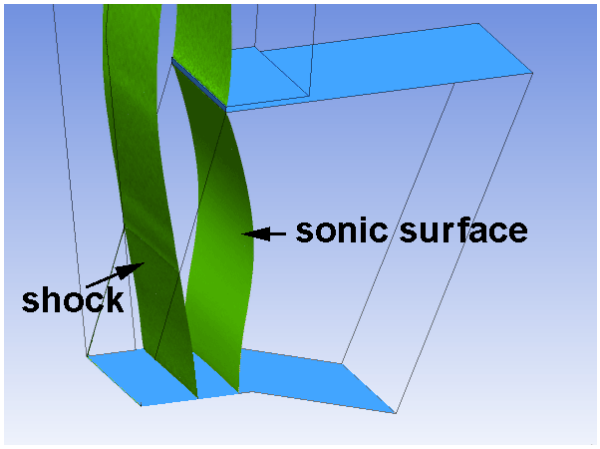

Figure-7. Surface $p(x,y,z)=p^*$ in 3D flow at M_∞=1.166, x_c=0.4, where the static pressure p^* is related to p_∞ and M=1 by the isentropic formula.

6. BEHAVIOR OF THE SHOCK GENERATED BY A BAR

Now we replace the plate (2) by a short bar of the same thickness

$$0.4<x<0.44, \quad 1<y<1.02, \qquad (8)$$

see Figure-8. Computations showed that the replacement entails only small changes in the shock location on the wall, cf. curves 1 and 3 in Figure-5.

The shock position as a function of the expansion corner angle θ turns out to depend crucially on the Mach number M_∞. If M_∞ =1.17, then the dependence $x_{sh}(\theta)$ is linear when θ increases from 0 to 2° (curve 1 in Figure-8). Meanwhile if θ further increases to 20°, then x_{sh} become almost fixed; the shock foot remains on the horizontal part of wall and does not reach the sonic line.

For M_∞ =1.175 and θ≥7°, transonic flow over the corner is non-unique, see curve 2 in Figure-9. Apart from the flow with a shock on the horizontal part of wall, there exists a flow regime with an oblique shock that reaches a vicinity of the expansion corner. The latter can be obtained by solving the problem with the uniform flow for initial data. The shock position x_{sh} persists when 7°≤ θ ≤ 20°. However, when θ becomes less than 7°, the supersonic region ruptures and the shock wave jumps upstream.

At M_∞ =1.18, if the expansion angle θ increases from 0 to 4.5° (curve 3 in Figure-9), then the shock shifts downstream, being located on the horizontal part of wall. However, when θ exceeds 4.5°, the shock jumps to the position x_{sh}≈0.363 and intersects the sonic line.

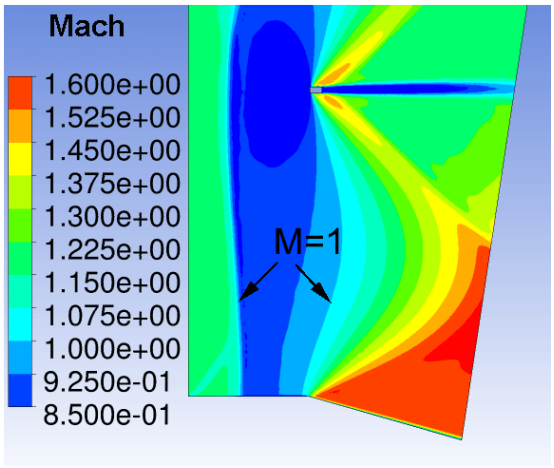

Figure-8. Mach number contours in 2D flow at M_∞=1.16, x_c=0.4. The plate (2) is replaced by the bar (8). The expansion angle is 16°.

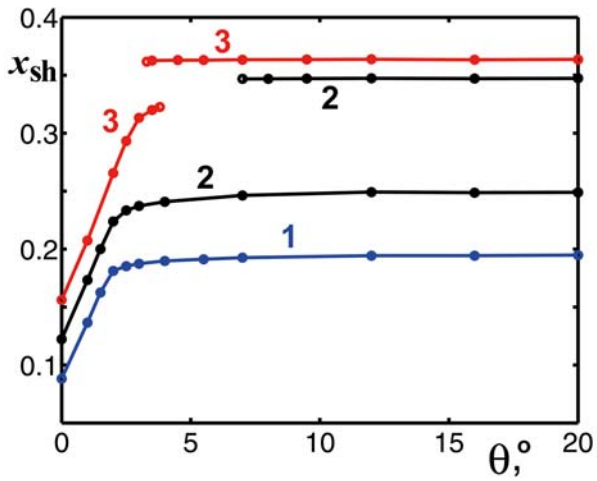

Figure-9. Shock wave coordinate x_{sh} versus the expansion corner angle θ in 2D flow at x_c=0.4. The plate (2) is replaced by the bar (8): 1 – M_∞ =1.17, 2 – M_∞ =1.175, 3 – M_∞ =1.18.

6. CONCLUSIONS

The numerical simulations of 2D shock wave behavior over an expansion corner showed the existence of corner angles and free-stream Mach numbers M_∞ at which there are abrupt jumps of the shock leg position. The flow hysteresis with respect to variation of M_∞ is small in contrast to transonic flow in channels with a slope of the upper wall [5, 6]. However, in a narrow range of M_∞, there exist non-unique solutions whose realization depends on the time history of boundary conditions. The shock instability is one of the key factors governing flow oscillations under unsteady perturbations in the free stream. Simulations of the 3D flow confirmed the findings.

ACKNOWLEDGEMENTS

This research was performed using computational resources provided by the Computational Center of St. Petersburg State University (http://cc.spbu.ru).

REFERENCES

[1] Jameson A. 1991. Airfoils admitting non-unique solutions of the Euler equations, AIAA Paper 91-1625. pp. 1-13.

[2] Kuzmin A. 2012. Non-unique transonic flows over airfoils. Computers and Fluids. 63. pp. 1-8.

[3] Kuzmin A., Ryabinin A. 2014. Transonic airfoils admitting anomalous behavior of lift coefficient. The Aeronautical J. 118(1202): 425-433.

[4] Ryabinin A. 2015. Transonic flow past symmetrical unswept and swept wings with elliptic nose. ARPN J. Engineering and Appl. Sciences. 10(20): 9359-9363.

[5] Kuzmin A. Shock wave bifurcation in channels with a bend. Archive Appl. Mech. 85(12). http://link.springer.com/article/10.1007/s00419-015-1062-z .

[6] Kuzmin A. 2016. Shock wave bifurcation in convergent-divergent channels of rectangular cross section. Shock Waves. pp. 1-6. http://link.springer.com/article/10.1007%2Fs00193-016-0624-5.

[7] Nakayama T., Sato T., Akatsuka M., Hashimoto A., Kojima T., Taguchi H. 2011. Investigation on shock oscillation phenomenon in a supersonic air inlet. AIAA Paper. 2011-3094. pp. 1-12.

[8] Hong W., Kim C. 2014. Computational studies on hysteretic inlet buzz characteristics under varying mass flow conditions. AIAA J. 52: 1357-1373.

[9] Menter F. R. 2009. Review of the Shear-Stress Transport turbulence model experience from an industrial perspective. Int. J. Comp. Fluid Dynamics. 23: 305-316.